Highly selective PdZn/ZnO catalysts for the methanol steam reforming reaction

Catalysis Science & Technology

ARTICLE

Highly selective PdZn/ZnO catalysts for the methanol steam reforming reaction

Ewa Nowicka,[a] Sultan M. Althahban,[b] Yuan Luo,[c] René Kriegel,[d] Greg Shaw,[a] David J. Morgan,[a] Qian He,[a] Masashi Watanabe,[b] Marc Armbrüster,[d] Christopher J. Kiely[a,b] and Graham J. Hutchings[*a]

One major drawback in the production of clean hydrogen from methanol is the formation of carbon monoxide which can subsequently act as a poison in fuel cell applications. Here we report on PdZn/ZnO catalysts developed for the methanol steam reforming reaction which have a high selectivity towards carbon dioxide. The impregnation-based method we employ for synthesising the PdZn/ZnO catalyst involves excess Cl^- anion addition to the metal chloride precursors which results in improved mixing of the metals. This subsequently leads to the formation of highly ordered PdZn alloy particles, which are responsible for high catalytic selectivity. This is contrary to the situation found for PdZn/ZnO catalysts prepared by more conventional Impregnation techniques (*i.e.,* without the addition of excess Cl^- anions), where random alloy PdZn particles were generated which result in a lower selectivity to CO_2.

Introduction

Methanol steam reforming (MSR) has gained much attention over recent years since it represents a viable method of producing pure H_2 for polymer electrolyte membrane fuel cells (PEMFCs). Although this reaction is very attractive, one of the reaction by-products, CO, is known to be a poison for Pt catalysts at the cathode even in very low (>10 ppm) concentrations.[1] MSR catalysts that give high selectivity towards CO_2 (*i.e.,* low selectivity towards CO) are therefore highly desired. Intermetallic PdZn catalysts have been extensively studied for this process, as they exhibit long term stability and low CO selectivity.[2-4] It has been shown that having PdZn is essential as monometallic Pd or Zn catalysts only exhibited poor selectivity to CO_2.[2, 5, 6] The high selectivity of PdZn has been assigned to the presence of oxidized Zn in the near-surface region. Armbrüster *et al*.[7, 8] investigated this phenomenon by correlating the selectivity displayed by the catalyst at different stages of the MSR reaction with high-resolution transmission electron microscopy (HRTEM) images. They concluded that *in-situ* partial oxidation of the PdZn nanoparticles leads to small ZnO surface patches, and also

inferred that the appearance of these oxidized Zn species is linked with high CO_2 selectivity.

The formation of the PdZn intermetallic compounds in Pd/ZnO catalyst materials has been investigated previously, especially in relation to varying key synthesis parameters such as the Pd:ZnO ratio, catalyst preparation method, support material and catalyst treatment conditions.[9-12] It was found that the catalytic function of the material increased markedly after a reduction pre-treatment which leads to formation of the intermetallic compound. Xiong *et al.*[13] reported that a ZnO supported PdZn catalyst which was synthesised by a hydrothermal method showed an activity increase of 53% in comparison to one prepared by impregnation using a commercial ZnO support. Chin *et al.*[9] investigated the role of the nitrate precursor during the preparation of a Pd/ZnO catalyst and found that the presence of nitrate anions (NO_3^-) altered textural properties such as porosity and crystallinity of the ZnO support. In addition, it affected the extent of intermixing occurring between the Zn^{2+} and Pd^{2+} species in the subsequent heat pre-treatment step, aiding the development of Pd-Zn interactions.[9] Since the presence of anions seems to play a very important role in the formation of PdZn alloys, we postulated that it might be desirable to utilise them to enhance the degree of mixing between the catalyst components in the preparation step. Sankar *et al.*[14] has previously reported the preparation of highly selective and stable AuPd/TiO$_2$ catalysts using chloride precursors along with an excess of chloride anions introduced by the addition of HCl. Catalysts prepared using such an 'excess anion' method displayed higher stability and better re-usability in the oxidation of alcohols as compared to materials synthesised without the addition of excess Cl^-.[15] It was postulated that the presence of the additional anions not only stimulates a better mixing between the metal precursors,

a. *Cardiff Catalysis Institute, School of Chemistry, Cardiff University, Main Building, Park Place, Cardiff, CF10 3AT, UK.*

b. *Department of Materials Science and Engineering, Lehigh University, 5 East Packer Avenue, Bethlehem, PA 18015-3195, USA.*

c. *Max-Planck-Institut für Chemische Physik fester Stoffe, Nöthnitzer Strasse 40, 01187 Dresden, Germany.*

d. *Faculty of Natural Sciences, Institute of Chemistry, Materials for Innovative Energy Concepts, Chemnitz University of Technology, 09107 Chemnitz, Germany*

* Correspondence to Graham J. Hutchings, e-mail: hutch@cardiff.ac.uk

but also limits agglomeration of the alloy particles after formation.

Here we report that by using this same 'excess anion' method of catalyst synthesis, highly selective PdZn/ZnO catalysts can be prepared for the methanol steam reforming reaction. It should be noted that replacement of HCl with other acids (*e.g.,* H_2SO_4, H_3PO_4) in the modified impregnation synthesis of the AuPd/TiO_2 system, lowered catalyst activity and selectivity.[14] Based on this prior work, we made the reasonable assumption that HCl would also be the optimum acid to use in the current PdZn/ZnO work.

Experimental

Catalyst Preparation

For the preparation of the 3%PdZn/ZnO catalysts used in this study, $ZnCl_2$ (≥98%, Sigma Aldrich) and $PdCl_2$ (≥99.9%, Sigma Aldrich) were used as metal precursors without further purification. Additional HCl was introduced in the form of a 0.58 M solution, prepared by the dropwise addition of 5 mL of concentrated HCl (37.2%, 12.1M) into 95 mL of an $PdCl_2$ aqueous solution (6 mg Pd /mL) under continuous stirring. The solution was left stirring for 16 h (at 500 rpm) at ambient temperature. For catalyst synthesis, the requisite amounts of aqueous Zn (6 mg/mL, 3.3ml) and Pd precursor solutions (6 mg/mL, 6.65ml) were charged into a 50 mL round-bottom flask containing deionized water (5 mL); samples with HCl added, were designated as a modified impregnation (M_{Imp}) catalysts, whereas those without HCl are termed as conventional impregnation (C_{Imp}) catalysts. The content of the flask was stirred vigorously (1000 rpm) and the temperature of the oil bath was raised from room temperature to 60°C over a period of 10 min. When a temperature of 60°C was reached, the ZnO support (1.94 g, Aldrich) was added slowly over an 8-10 min period with constant stirring. The pH of the solution was analysed continuously using a Toledo pH meter. When addition of the support material was complete, the slurry was stirred at 60°C for an additional 15 min and then the temperature of the oil bath was raised to 95°C, and the slurry was stirred overnight until all the water had evaporated leaving a dry solid. This solid powder was subsequently transferred into a mortar and pestle and was ground thoroughly. For the preparation of acid treated ZnO support materials, 6.65 ml of 0.58 M aqueous HCl was added to a round bottom flask containing 8.3 ml water under vigorous stirring conditions. Next, 1.96 g of ZnO was added to the mixture and stirred at room temperature and the subsequent synthesis steps remained the same as for the standard preparation procedure described above. Finally, the catalyst was pre-treated in the methanol steam reforming (MSR) reactor under a steady flow of 5% H_2 in Ar for 4 h at 500 °C with a heating rate of 10°C/min.

Methanol Steam Reforming

Methanol steam reforming tests were carried out using powder catalyst samples (150 mg) in a plug flow reactor (inner diameter 7.9 mm, silica coated stainless steel) which was mounted inside a hot box (120 °C) to prevent condensation of liquids (MicroActivity, PID Eng & Tech). The catalysts were not exposed to air after calcination and reduction treatments. The MSR feed consisted of 0.0325mL/min liquid (50 mol% MeOH 0.0225mL/min (Sigma-Aldrich, ≥ 99.9%)), 50mol% deionized water (0.01mL/min), 38.7 ml/min N_2 (99.999%, Praxair) and 4.6 mL/min He (99.999%, Praxair). N_2 was used as a carrier gas, while He was used as an inert tracer gas to calibrate the volumes of the gaseous products, since residual MeOH and H_2O are not determined in the effluent. The gas composition in the product stream was determined every 4 min by gas chromatography (Varian Micro GC CP4900), which allowed for quantitative determination of CO with a detection limit down to 20 ppm. Furthermore, all gaseous reactants and products were monitored by a mass spectrometer (Pfeiffer, Omnistar 300). It was not possible to directly determine the amount of unconverted MeOH or H_2O by either GC and MS analysis, because the product gas was dried using a cooling trap and a subsequent Nafion® membrane before any gas phase analysis. For the MSR measurements, a maximum reaction temperature of 300 °C was employed. An isothermal test of 10 h duration was carried out directly after a series of temperature dependent measurements including temperature changes from 150 °C to 300 °C and 175 °C to 300 °C (using a heating and cooling rate of 10°C/min).

Catalyst Characterization

BET Surface Area Measurement

BET surface area analysis was carried out using a Quantachrome Quadrasorb evo system. A 5-point analysis was performed using N_2 as the adsorbate gas. Samples were degassed in vacuum for 1 h at 120 °C prior to analysis.

In-situ XRD

XRD analysis was conducted using a PANalytical X'pert Pro diffractometer employing a Cu K_α X-ray source. Typical scans were taken over a 2θ angular range between 10 and 80° using 40kV and 40mA X-ray source settings. Catalyst samples were heated to 500 °C under a constant flow of 5% H_2/N_2 (20 mL/min) and scans were taken at 100 °C temperature intervals.

H$_2$-Temperature-Programmed Reduction (TPR)

TPR analysis was carried out on a Thermo TPD/R/O 1100 series instrument equipped with a thermal conductivity detector (TCD). The catalyst (50mg) was heated up to 600 °C under an atmosphere of 10% H_2/Ar (5 °C/min) after pre-treatment in Ar at 110 °C for 45 min.

X-Ray Photoelectron Spectroscopy (XPS)

XPS was performed on a Thermo Scientific K-alpha+ photoelectron spectrometer, using monochromatic Al K_α radiation. High resolution and survey scans were performed at pass energies of 40 and 160eV, respectively. Charge compensation was achieved using a combination of low energy electrons and argon ions. The Zn(2p$^{3/2}$) signal was chosen as the calibration point, with all samples exhibiting this peak at 1021.9

eV and consistent with the negligible binding energy shift between Zn(0) and Zn(II) oxidation states.[16]

Scanning Transmission Electron Microscopy (STEM)

Samples for examination by STEM were prepared by dry dispersing the catalyst powder (reduced at 500 °C) onto a holey carbon film supported by a 300-mesh copper TEM grid. Bright field (BF) and high angle annular dark field (HAADF) STEM images were taken using an aberration corrected JEM ARM-200CF microscope operating at 200kV. This instrument was also equipped with a JEOL Centurio silicon drift detector for X-ray energy dispersive spectroscopy (XEDS). Particle size distribution histograms were generated by analysis of representative HAADF electron micrographs using ImageJ.

Results and Discussion

In our previous work,[14] we showed that AuPd/TiO$_2$ catalysts prepared by addition of excess chloride ions to the precursor metal salts produced materials with increased catalytic activity for benzyl alcohol oxidation and H$_2$O$_2$ synthesis. The additional presence of ions during the preparation step was shown to improve the mixing of the metal precursor salts to facilitate the formation of a more homogenous mixture of metal ions, thereby enabling improved dispersion during the impregnation stage. We used the same methodology for preparation of our Pd-Zn/ZnO materials, aiming to achieve more uniform PdZn alloys that might lead to higher selectivity in the MSR reaction. It should be noted that most conventional routes for preparing Pd/ZnO catalysts for methanol steam reforming usually rely upon a single Pd(NO$_3$)$_2$ precursor. Furthermore, it was found that a highly acidic Pd precursor could affect the extent of mixing between ZnO and Pd^{2+}.[8, 9] Since the mixing between the metallic elements should be optimised, we decided to introduce a separate Zn precursor (ZnCl$_2$) instead of just relying, as is usually the case, on interaction of deposited Pd with the underlying ZnO support. Such a method of pre-mixing Pd and Zn precursors to form intermetallic PdZn nanoparticles has been reported previously on CeO$_2$.[10] Similarly, PdZn alloys have been synthesised on supports such as TiO$_2$ or Al$_2$O$_3$ by chemical impregnation methods.[17] In addition, we compared materials prepared *with* (M$_{Imp}$ route) and *without* (C$_{Imp}$ route) the addition of excess HCl as a mixing facilitator. The resulting catalyst materials were then assessed for their efficacy in the methanol steam reforming reaction.

It should be noted that during the catalyst preparation procedure, changes in the pH of the precursor mixture and ZnO were continuously monitored. For the catalysts prepared by the standard impregnation C$_{Imp}$ route, the pH of the PdCl$_2$, H$_2$O and ZnCl$_2$ mixture was 1.5. In the M$_{Imp}$ case, the solution obtained from mixing PdCl$_2$ (containing 0.58 M HCl), ZnCl$_2$ and additional H$_2$O resulted in a pH value of 0.33. After addition of 1.98 g of ZnO, the pH value in the M$_{Imp}$ case rose to 6.1, whereas for the C$_{Imp}$ catalyst it increased to 6.3. Hence, there was no significant difference in the pH level of the slurries prepared by the M$_{Imp}$ and C$_{Imp}$ methods.
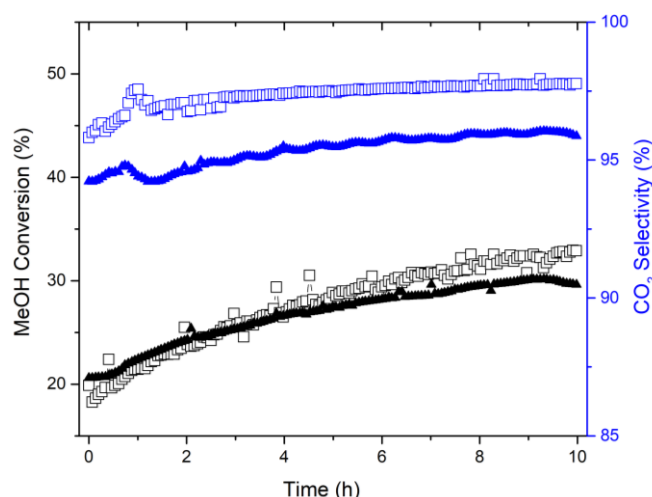

Figure 1. Methanol conversion and CO$_2$ selectivity of freshly reduced 3%PdZn/ZnO MSR catalysts measured under isothermal conditions at 300 °C. *Key:* M$_{Imp}$ materials prepared with 0.58M HCl (□); C$_{Imp}$ material prepared without additional HCl (▲).

For comparison of the catalytic activity of materials made by the M$_{Imp}$ and C$_{Imp}$ routes, a common nanopowder zinc oxide support was used (Aldrich, 10.8 m^{2}g^{-1}) as it is well known that the surface area can influence the catalytic activity.[13] First, we investigated the role of excess Cl$^-$ anions in the preparation by testing the catalysts prepared with and without HCl. The MSR performance for each material was measured at 300 °C over a period of 10 h as shown in Figure 1.

Both catalysts displayed similar activity levels in terms of methanol conversion, especially at the beginning of the reaction. It is worth emphasizing that the conversion increased by 15% in the case of the M$_{Imp}$ catalyst over the 10 h duration of the test and the productivity increased from 754 to 1297 mmol H$_2$ per mmol Pd per h. A similar effect, although less pronounced, was also observed for the C$_{Imp}$ material and resulted in a conversion increase of 10% over 10 h. These results strongly suggest that the catalyst material is undergoing some beneficial physical changes under the MSR reaction environment.

A similar general trend of improving behaviour was observed in the selectivity of the catalysts, which increased with time-on-line for both the M$_{Imp}$ and C$_{Imp}$ 3%Pd-Zn/ZnO materials. However, it should be noted that the catalyst synthesized by the modified impregnation route out-performed its counterpart prepared by conventional impregnation and resulted in a significantly higher selectivity to CO$_2$. The high selectivity to CO$_2$ is not limited at this reaction temperature and at the MeOH conversion achieved, as shown by the equilibrium calculations presented in Figure S1 (Supplementary Information). The gradual improvement in catalytic performance with time-on-line in terms of both conversion and selectivity might be related to a structural modification of the materials under reaction conditions. For instance, Friedrich *et al.*[7] and Heggen *et al.*[8], using variety of *in-situ* microscopy techniques, have previously demonstrated that discrete ZnO patches can form on the supported PdZn intermetallic metal particles during catalyst operation. They also convincingly showed that direct oxidation

Table 1. Influence of support treatment on catalytic activity using bare ZnO.

Treatment	Conversion (%)	Selectivity CO_2 (%)	Productivity (mmol H_2 $g_{cat}^{-1}h^{-1}$)
H_2O	2	100	2.118
HCl*	0.1	100	0.023

Reaction conditions: ZnO 1g, T = 300 °C, MeOH 0.0225ml/min, H_2O 0.01ml/min, N_2 38.671ml/min. *ZnO washed with 0.058M HCl, 2g used in the reaction.

Table 2. Surface area and crystal size measurements for the fresh ZnO support and the M_{Imp} and C_{Imp} derived 3%PdZn/ZnO catalysts.

Catalyst	Treatment	Mean ZnO crystallite size (nm)	S_{BET} (m^2g^{-1})
ZnO	Fresh	44	10.8
3% Pd-Zn/ZnO (no HCl)	Fresh	46	*N/A*
	Reduced	44	10.9
3% Pd-Zn/ZnO (HCl)	Fresh	58	*N/A*
	Reduced	54	4.6

of the PdZn particles occurs, as opposed to migration of ZnO support material over the surface of the PdZn particles. However, it should be noted that their catalyst originated from a monometallic Pd on ZnO material, whereas our M_{Imp} and C_{Imp} catalysts were prepared by co-impregnation of Pd and Zn precursors onto the ZnO support material.

It is interesting to compare the activity of our catalysts with other literature reports. The M_{Imp} 3%Pd-Zn/ZnO catalyst showed an activity of 1297 mmol H_2 per mmol Pd per h, while the C_{Imp} variant gave an activity of 1126 mmol H_2 per mmol Pd per h. These activity levels look very promising compared to the 319 mmol H_2 formed using a 9.2%Pd/ZnO catalyst as reported by Heggen *et al.* [8]

Our primary motivation for creating excess Cl^- ions via the addition of HCl was to ensure efficient and proper mixing of the metal precursors, however, it was also important to ascertain if these residual Cl^- ions themselves affected the catalytic activity. We investigated this possibility by examining pure ZnO materials treated with H_2O and HCl (see Table 1).

Lorenz *et al.* [18] have reported that ZnO itself is highly selective towards CO_2 when used as an MSR catalyst. Their fresh ZnO material gave 99.6% selectivity to CO_2 and 3.6% methanol conversion (0.63 mmol H_2 g_{cat}^{-1} h^{-1}). By comparing their data to that which we obtained using H_2O and HCl-treated ZnO for the MSR reaction (Table 1), it is clear that washing with H_2O does not have a negative effect on catalyst selectivity or activity. However, the treatment of bare ZnO with HCl led to a decrease in the conversion suggesting that the presence of residual Cl^- ions alone could be detrimental for this reaction. Nevertheless, we show that they may play a beneficial role in the PdZn/ZnO system, as the catalyst prepared with excess of HCl outperformed its counterpart prepared by the conventional impregnation method in the methanol steam reforming reaction.

Catalyst Characterization

It has also been previously reported that the surface area of the ZnO support plays an important role in determining MSR catalyst activity.[19] Table 2 summarises the surface areas and mean particle size of the bare nano-powder ZnO as well as the M_{Imp} and C_{Imp} derived 3%PdZn/ZnO catalysts. The mean crystallite size was determined by profile fitting the FWHMs of all the ZnO XRD peaks using the Scherrer equation. The ZnO in the M_{Imp} derived catalyst was found to have a significantly lower surface area and larger mean particle size than either the C_{Imp} catalyst or bare ZnO support material, and so might simplistically be expected to have a worse activity if surface area were the dominant parameter affecting catalytic performance. The fact that we see better catalytic performance for the M_{Imp} 3%PdZn/ZnO materials, despite it having the lowest ZnO surface area, means that some other factors besides surface area must be coming into play.

It might be anticipated that the modification of ZnO with HCl would lead to the undesired changes in the catalyst structure, which has led to a definite preference in the literature for preparing these PdZn catalysts using organic precursors.[20] However, the acid treatment in our case, followed by reduction with 5% H_2/Ar for 4 h at 500°C, seems to be beneficial as our M_{Imp} 3%PdZn/ZnO catalysts displayed higher selectivity when compared with conventionally impregnated material and previously reported Pd/ZnO derived catalysts.[7]

X-ray Diffraction

The structure of both M_{Imp} and C_{Imp} derived catalysts during the reduction treatment were studied by *in-situ* XRD measurements (Figure 2). The fresh C_{Imp} PdZn/ZnO sample prepared by conventional impregnation showed peaks consistent with the hexagonal ZnO phase. In contrast the samples prepared by modified Impregnation contained a significant amount of Simonkolleite (ICSD No. 77-2311) in addition to the expected ZnO phase. Simonkolleite is a hydrated zinc hydroxide chloride compound ($Zn_5Cl_2H_{10}O_9$) which can form when HCl is added to ZnO during the M_{Imp} synthesis
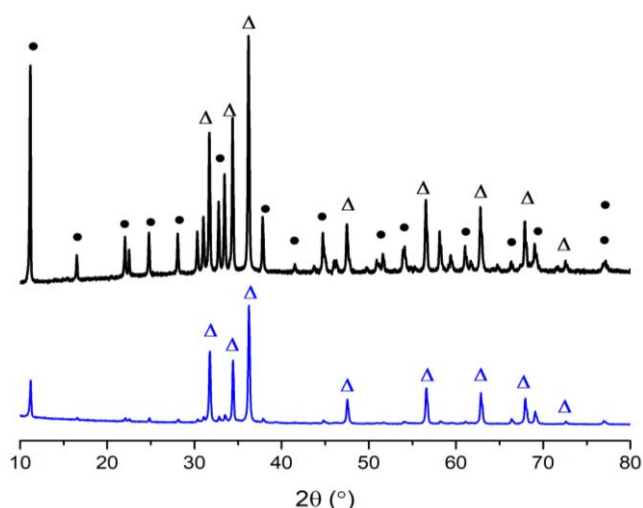
Figure 2. XRD patterns of M_{Imp} derived 3%Pd-Zn/ZnO (top) and C_{Imp} derived 3%Pd-Zn/ZnO (bottom), in the unreduced state, analysed at 25°C. *Legend* ● symbols indicate reflections from $Zn_5Cl_2H_{10}O_9$, while Δ symbols are reflections from ZnO.

Figure 3. XRD patterns of M_{Imp} derived 3%PdZn/ZnO (top) and C_{Imp} derived 3%PdZn/ZnO (bottom) materials after reduction in 5% H_2/N_2 at 500°C. *Legend:* ♦ symbols indicate reflections from tetragonal PdZn, while Δ symbols are peaks from ZnO.

procedure. This same phase was also observed in the pure ZnO material treated with HCl (Figure S2 – Supplementary Information). Interestingly, no Pd-containing phase was observed in the XRD pattern for the fresh M_{Imp} PdZn/ZnO catalyst, which might imply the formation of a Pd-containing Simonkolleite phase, which could act as a single-source precursor phase for subsequent PdZn intermetallic particles.

Heat treatment of these materials under reducing conditions (*i.e.,* heating from 25°C to 500°C in 10% H_2/N_2) led to significant changes in their XRD patterns (Figure 3). The reflections assigned to the Simonkolleite phase in the M_{Imp} 3%PdZn/ZnO catalyst gradually decreased in intensity and eventually disappeared altogether. The final M_{Imp} 3%PdZn/ZnO catalyst was found to consist of the ZnO support phase along with some tetragonal PdZn (ICSD 180143) alloy particles as evidenced by very weak 111 and 200-type reflections at 2Θ = 41.26° and 44.04° respectively. The corresponding XRD pattern for the *in-situ* reduced counterpart C_{Imp} 3%PdZn/ZnO catalyst showed the expected ZnO reflections, but also developed weak peaks at 2Θ = 41.42 ° and 44.31° corresponding the (111) and (200) planes of the tetragonal PdZn alloy phase. It is therefore postulated that under reducing conditions, Simonkolleite undergoes decomposition, which can then easily lead to the formation of a PdZn alloy. The formation of PdZn alloys when starting from Pd/ZnO requires first the reduction of Pd and then formation of PdH_x. It has been reported that the strong interaction between metallic palladium or palladium hydride and the support leads to hydrogen spill-over during reduction.[21] This enables the reduction of the ZnO in the vicinity of the Pd particles and the formation of the intermetallic PdZn compound at lower reduction temperatures.

XRD analysis confirmed the presence of the tetragonal PdZn phase in both the reduced M_{Imp} and C_{Imp} derived catalysts, but the reflections are relatively weak as the PdZn content is low (<3%). In both materials, the PdZn alloy phase was found to form at a reduction temperature somewhere between 300°C
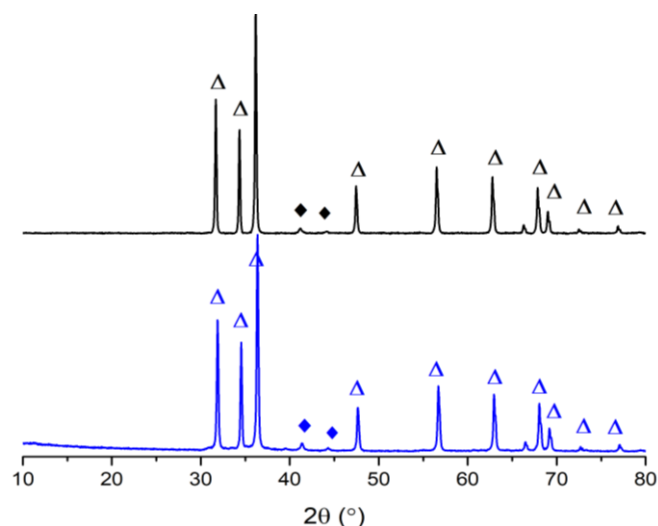
and 400°C (Figure 4) which is in good agreement with expected literature values.[22] It should also be noted that no reflections in either sample could be ascribed to the presence of monometallic Pd or Zn.

Temperature Programmed Reduction

Figure 5 shows temperature-programmed reduction (TPR) profiles for the fresh M_{Imp} and C_{Imp} derived 3%PdZn/ZnO catalysts as well as for fresh and HCl treated bare ZnO nano-powder supports. Positive peaks in a temperature range from 100 to 300°C were observed in the TPR traces for both the M_{Imp}
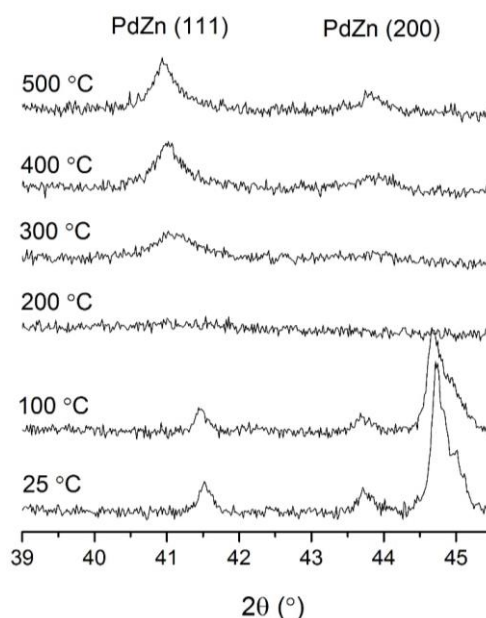

Figure 4. *In-situ* XRD patterns of the M_{Imp} derived 3wt%PdZn/ZnO catalyst: *in-situ* analysis under reducing conditions (5% H_2/N_2; 20 ml/min) at several temperatures ranging between 25 and 500°C (Reflections at 41.43°, 43.67° and 44.69° are assigned to $Zn_5Cl_2H_{10}O_9$).
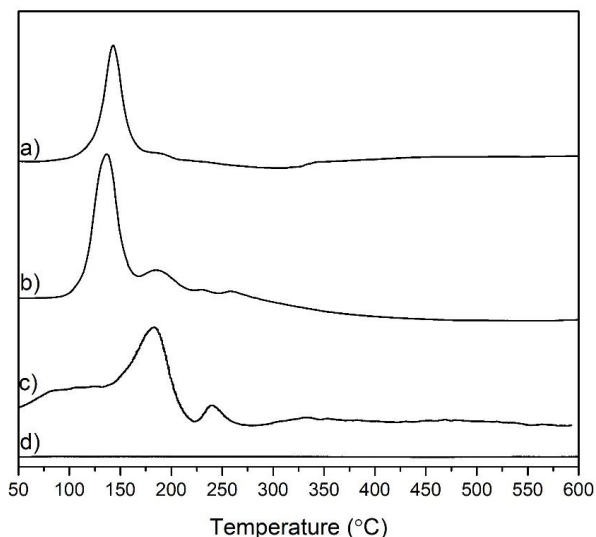
Figure 5. TPR profiles for (a) the C_{Imp} 3%ZnPd/ZnO catalyst, (b) the M_{Imp} 3% ZnPd/ZnO catalyst (c) the HCl treated ZnO support and (d) the fresh untreated ZnO support.

and C_{Imp} catalysts and from the HCl treated ZnO support material. By way of contrast, the TPR trace for the untreated ZnO sample was essentially featureless. Both the M_{Imp} and C_{Imp} catalysts (Figures 5a and b) show a first reduction peak just above 120°C (*i.e.*, 136°C for M_{Imp} PdZn/ZnO and 143°C for C_{Imp} PdZn/ZnO). A second, well distinguished peak was observed at 185°C for the M_{Imp} PdZn/ZnO catalyst, which was largely absent
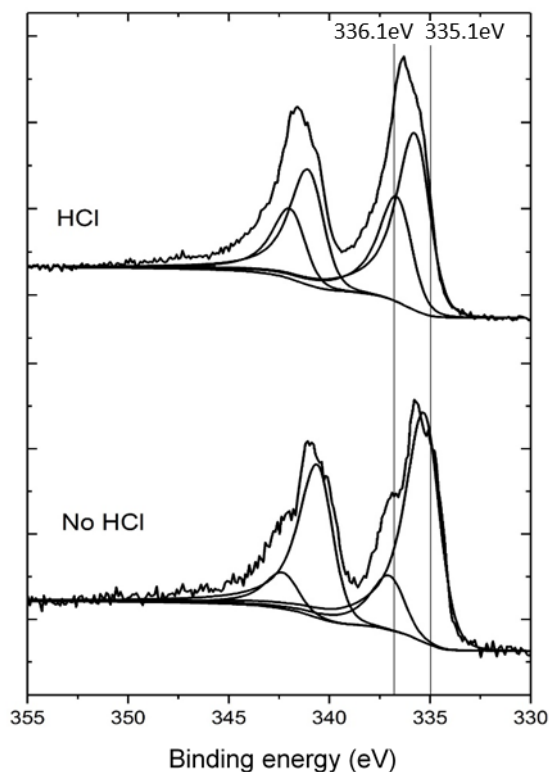
in the material prepared by the C_{Imp} method. TPR analysis of the HCl treated ZnO (Figure 5c), showed a comparable pattern of higher temperature reduction peaks to the M_{Imp} catalyst, suggesting that similar species were present in these two materials. As both these samples also displayed similar XRD patterns, with many of the reflections being assigned to the Simonkolleite phase, it is therefore likely that the TPR features above 150°C, arise from the reduction of Simonkolleite species. It is also plausible that a Pd-containing version of the Simonkolleite phase may be present in the M_{Imp} PdZn/ZnO sample which plays an important role in the subsequent formation of PdZn intermetallic compounds.

XPS analysis

XPS analysis (Table 3) showed that the apparent surface concentration of Pd for both the M_{Imp} and C_{Imp} catalysts decreased following reduction at 500 °C. This change is concomitant with a downward shift in the binding energy of the Pd(3d) peaks from 337.4 eV (characteristic of Pd-Cl) in the fresh samples, to *ca.* 336 and 335 eV in the reduced ones (Figure 6, Figures S3 and S4 – Supplementary Information). The binding energy values of Pd ($3d_{5/2}$) for PdZn alloys have been reported[23,24] to vary from 335.1 to 336.2 eV; however, it is also accepted that alloying Pd with Zn increases the binding energy of the Pd ($3d_{5/2}$) signal as a consequence of charge transfer and re-hybridisation.[25]
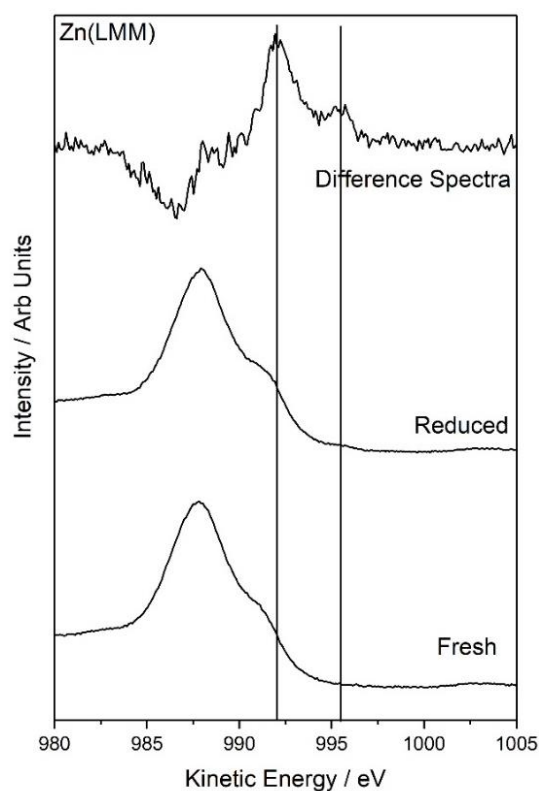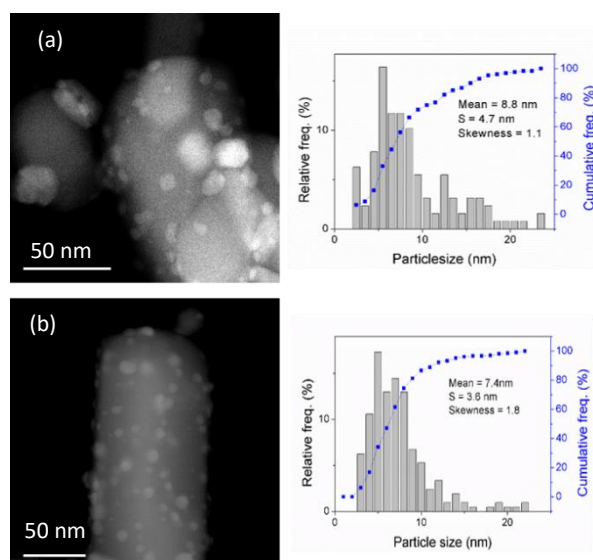

Figure 6. The Pd(3d) XPS spectra for reduced M_{Imp} derived (above) and C_{Imp} derived (below) 3%PdZn/ZnO catalysts.

Figure 7. Zn (LMM) X-ray excited Auger electron spectra for the fresh and reduced variants of the M_{Imp} derived 3%PdZn/ZnO catalyst. The difference spectrum between the fresh and reduced sample is also plotted.

Table 3. XPS analysis of the M_{Imp} and C_{Imp} derived 3%PdZn/ZnO catalysts in the fresh and reduced states.

Catalyst		Concentration (at %)			
		Pd	Zn	Cl	O
C_{Imp}	fresh	2.9	47.3	2.6	47.2
3%PdZn/ZnO	reduced	2.3	44.0	3.4	44.5
M_{Imp}	fresh	5.4	34.9	4.7	48.0
3%PdZn/ZnO	reduced	3.8	39.2	4.7	43.9

Figure 8. Representative STEM-HAADF images and the corresponding particle size distributions (PSDs) of (a) the C_{Imp} 3%PdZn/ZnO catalyst and (b) the M_{Imp} 3%PdZn/ZnO catalyst.

We interpret the signals at *ca.* 335 and 336 eV as being either associated with discrete PdZn alloy particles of differing composition, or due to a surface enrichment of the PdZn nanoparticles with Pd caused by interaction with the atmosphere as the samples were handled *ex-situ* in air prior to analysis. The possibility of larger metallic Pd particles being present (with an expected binding energy *ca.* 335 eV) can be discounted in our M_{Imp} and C_{Imp} samples as (i) no characteristic Pd reflections were observed in the XRD spectra and (ii) the high selectivity of our catalysts to CO_2 strongly suggests the absence of metallic Pd.[26] In addition, we investigated the Zn (LMM) X-ray excited Auger emission spectra (XAES) for the fresh and reduced variants of the M_{Imp} derived 3%PdZn/ZnO sample. The difference spectrum between the fresh and reduced sample is also plotted to improve the visibility of the weak shoulder feature (Figure 7). Despite no observable broadening of the $Zn(2p_{3/2})$ core-level, alloying of Pd and Zn is supported by the emergence of a new state in the Zn (LMM) XAES spectrum, characterised by a major peak at 992.1 eV, which corresponds to a modified Auger parameter of *ca.* 2014 eV and is characteristic of metallic Zn or Zn-containing alloys.[16,27]
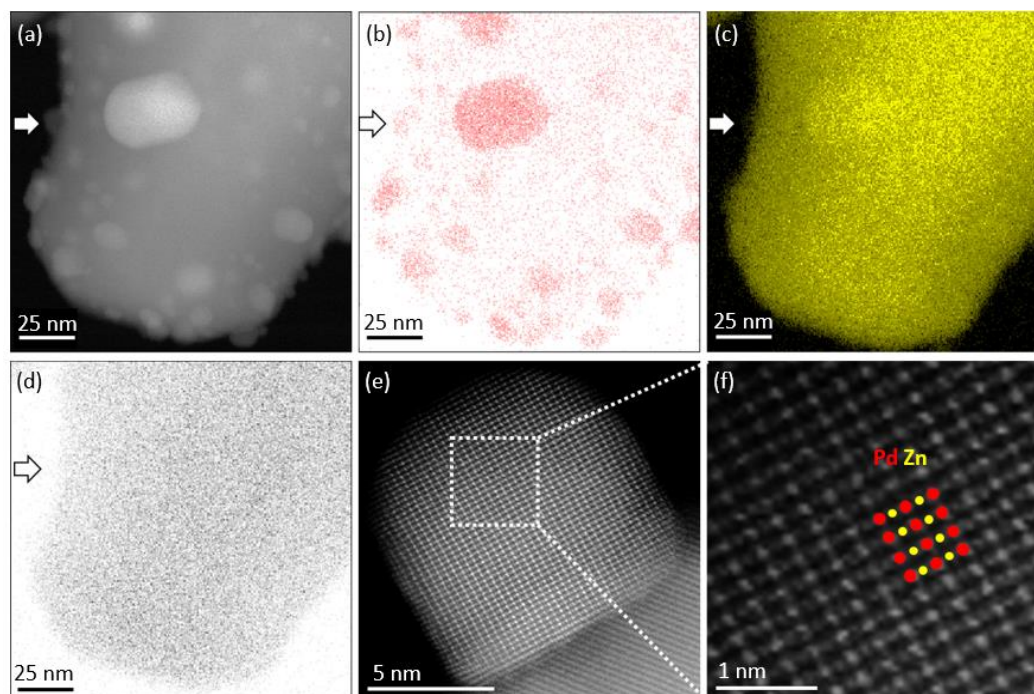
Figure 9. STEM-XEDS elemental maps and STEM-HAADF imaging of the M_{Imp} 3%PdZn/ZnO catalyst. A STEM-HAADF image of the catalyst is shown in (a) along with the corresponding XEDS elemental maps of (b) Pd, (c) Zn and (d) O. The intermetallic particles in profile indicated by arrows in (a-d) show the presence Zn and Pd but not an O signal. (e) A higher magnification STEM-HAADF image of a PdZn particle, showing characteristic L1$_0$ ordering of Pd and Zn atoms. This can be better seen in the magnified view in (f), which is overlaid with the atomic structure of PdZn (ref ICSD 180143) viewed along the [110] projection.

It is also clear from the XPS data shown in Table 3 that the 4 h reduction treatment of the catalyst in 5% H_2/Ar at 500°C did not result in the removal of chloride species from the M_{Imp} and C_{Imp} catalysts, since a detectable concentration of Cl^- remained. The apparently slighter higher concentration of Cl present after reduction for the C_{Imp} catalyst could be due to strong anchoring of Cl to the substrate, resulting in a higher apparent dispersion of Cl after alloying and the associated particle size changes under the reductive atmosphere. This can be supported by analysing the binding energy of *ca. 199 eV*, that is typical for metal-Cl bonds.[16] Since a significant quantity of surface Cl^- was detected by XPS even after reduction step, it is therefore valid to consider the possible role of residual Cl^- species in the methanol steam reforming reaction. As the MSR reaction was taking place at 300 °C it is very unlikely that Cl^- would be removed from the catalyst surface at a temperature lower than that of the reduction step (500 °C) during which the Cl^- anions are known to remain on the surface. Also, taking into account the experimental data provided in Table 1, it is unlikely that Cl^- will have a positive effect on the catalytic activity. To address this aspect further additional STEM-XEDS studies on these catalyst samples were performed.

Electron Microscopy Analysis

Representative STEM-HAADF images of the unused C_{Imp} and M_{Imp} derived 3%PdZn/ZnO catalysts are presented in Figures 8(a) and 8(b) respectively. As expected, the ZnO support grains,

because they were of the same origin, were very similar in each case, being in the 50 – 200 nm range. The metal nanoparticles were homogeneously dispersed on the ZnO support grains in both cases, but the particle size distribution of each was slightly different. For the M_{Imp} 3%PdZn/ZnO sample, the metal particles range from 3 to 22 nm in size, with the mean size being ~7.5 nm. The corresponding C_{Imp} derived 3%PdZn/ZnO sample displayed a slightly broader metal particle size range (3 to 25 nm) with a higher population of the bigger particles and a larger mean metal particle size of ~8.8 nm.

Additionally, STEM-XEDS analysis was attempted to see if any significant residual Cl^- is retained in our M_{Imp} and C_{Imp} derived PdZn/ZnO catalysts (Figures S5 and S6, Supplementary Information). In both cases the measured XEDS intensity of the Cl mapping signal was quantitively in the noise level (1-3 counts only) and no identifiable Cl peak could be found in integrated point spectra. Therefore, the Cl content is below the detectability level of the XEDS technique, which is ~0.5 wt%. The discrepancy between the EDS and XPS analysis is related to the sampling depth for each technique. While the STEM-XEDS is effectively sampling the bulk of PdZn/ZnO particles, the XPS method is sampling only the first few nm. It is therefore probable that less than 0.5 at% Cl is present in total, but as it is concentrated on the catalyst surface then XPS analysis can detect its presence as noted in Table 3. It is therefore likely that the surfaces of both the M_{Imp} and C_{Imp} catalysts have a partial Cl^-coverage, which is not removed during the reduction step.
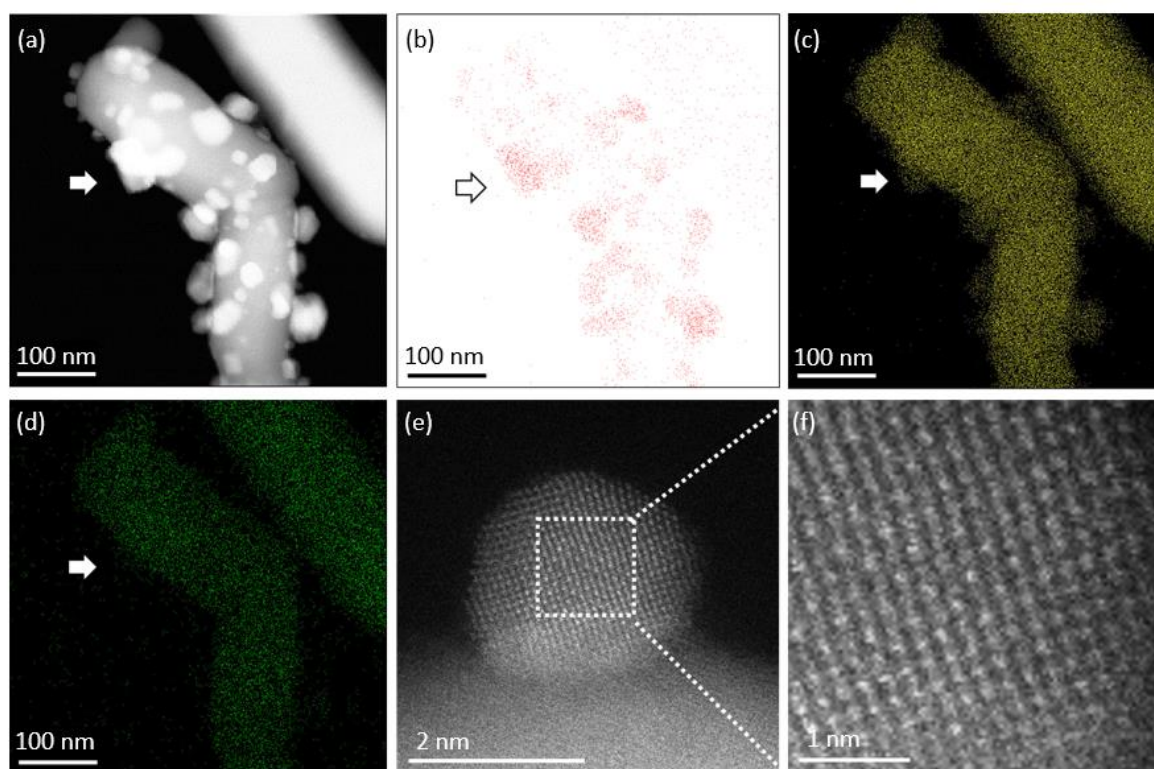

Figure 10. STEM-XEDS elemental mapping and STEM-HAADF imaging of the C_{Imp} 3%PdZn/ZnO catalyst. A lower magnification STEM-HAADF image of the catalyst is shown in (a) along with the corresponding XEDS elemental maps of (b) Zn, (c) Pd and (d) O. The intermetallic particles in profile indicated by arrows in (a-d) show Zn and Pd signals but not any O. (e) A higher magnification STEM-HAADF image of a PdZn particle, showing the ($L1_0$) tetragonal PdZn phase. (f) A higher magnification HAADF image of a [001] projection of a PdZn.
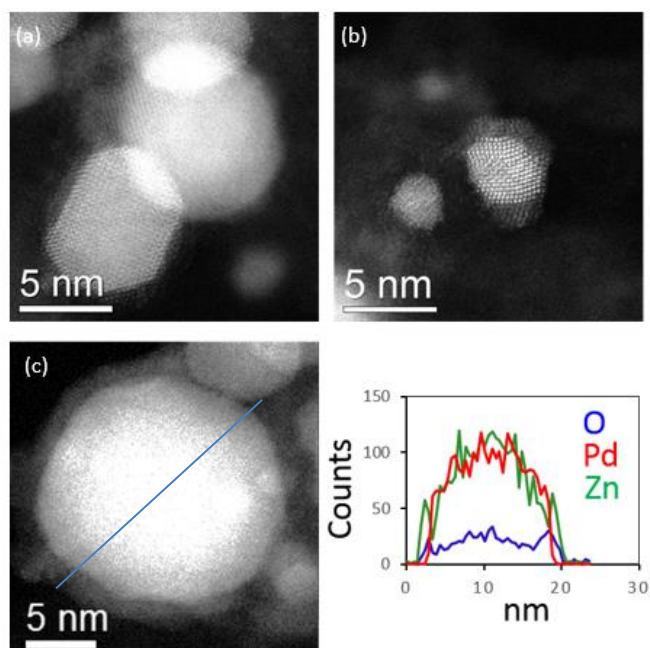
Figure 11. (a, b, c) Representative HAADF images of some PdZn intermetallic particles in the M_{Imp} derived 3%PdZn/ZnO catalyst after use, showing that they are no longer atomically clean, but are now decorated with a 1-2 nm thick patchy overlayer whose average mass is less than that of the PdZn particle. The XEDS line-scan in (d) was acquired along the blue line shown on the particle in (c) and shows that the surface is enriched in Zn and deficient in Pd, implying the formation of a ZnO-like surface overlayer.

The compositions of individual supported metal nanoparticles were also probed using STEM-HAADF imaging and X-ray energy dispersive spectroscopy (XEDS), and the results are shown in Figures 9 and 10 for the M_{Imp} and C_{Imp} derived 3%PdZn/ZnO catalysts, respectively. The metal particles examined on both catalysts were all found to be PdZn alloys, as evidenced by the presence of both Pd and Zn signals in XEDS maps of particles oriented in profile view at the edge of the ZnO support, (which are highlighted with arrows in Figures 9 (a-d) and Figures 10 (a-d)). Higher magnification atomic resolution STEM-HAADF images of representative PdZn particles for the two catalysts are shown in Figures 9 (e, f) and 10 (e, f). Measurement of lattice spacings and interplanar angles confirmed the supported alloy particles in both cases to have a tetragonal structure consistent with PdZn (ICSD 180143) which is known to exist for alloy compositions containing between 38 and 50 at% Zn. In the M_{Imp} derived catalysts the PdZn particles when viewed along certain crystal projections (*e.g.,* [010] and [110]) showed strong and distinct periodic mass contrast in HAADF images that is consistent with $L1_0$ type ordering of Pd and Zn atoms on alternate atomic columns. To illustrate this atomic ordering more clearly, Figure 9(f) shows a magnified [110] HAADF projection view of the atomic structure in Figure 9(e) with the theoretical atomic structure projection of $L1_0$ type PdZn superimposed on top of the experimental image. A distinct difference noted in the C_{Imp} derived 3wt% PdZn/ZnO catalysts was that the vast majority of the PdZn alloy particles, while showing a tetragonal structure, did not show the high

degree of ordering on the Pd and Zn sub-lattices that was found for the M_{Imp} derived materials (Figures 10 (e, f)).

The M_{Imp} 3wt%PdZn/ZnO material was also examined after 10 h use as an MSR catalyst. As shown in Figure 11, the catalyst structure was significantly modified during the activation and use process. The supported PdZn alloy particles were no longer atomically clean but became decorated with a 1-2 nm thick patchy overlayer whose average mass is less than that of the underlying PdZn particle (Figures 11(a-c)). The XEDS line-scan shown in Figure 11 (d) was acquired along the blue line indicated on the particle in Figure 11 (c) and shows that the surface is enriched in Zn and deficient in Pd, implying the formation of a ZnO-like surface overlayer. It is unclear if this overlayer originates from (i) preferential Zn oxidation in the PdZn particle surface or (ii) ZnO migrating from the support over the PdZn particle via a strong metal support interaction (SMSI) effect. The existence of ZnO islands on the PdZn particle surface is however entirely consistent with previous reports from Armbruster *et al* who associated this morphology with fully active catalysts.[7, 8] The time needed to develop this overlayer also seems to correlate with the induction period required for this PdZn/ZnO catalyst to reach its full activity.

Conclusions

A 3% PdZn/ZnO catalyst has been synthesized using a modified impregnation (M_{Imp}) technique in which excess Cl^- ions were introduced along with the metal precursor salts. As a result, a highly selective catalyst for the methanol steam reforming reaction was obtained. The origin of the high selectivity to CO_2 lies in the lack of monometallic Pd and the efficient formation of homogeneously distributed and structurally ordered PdZn intermetallic particles. This desirable nanostructure was achieved by the efficient mixing between the metal chloride precursors occurring as a result of HCl addition and perhaps the formation of a mixed cation compound resembling a Pd-containing Simonkolleite phase. This is further supported by comparisons with the corresponding catalyst prepared by a more conventional impregnation method which was comprised of larger random alloy PdZn particles and exhibited a lower selectivity towards CO_2. It is believed that the main contributor to improvement of catalytic activity observed for both the M_{Imp} and C_{Imp} materials with time-on-line is the formation of nanoscale ZnO islands on the surface of PdZn particles. However, the role of residual Cl^- present in the catalyst and its influence on catalytic activity still needs further investigation and should not be excluded from consideration.

Conflicts of interest

There are no conflicts to declare.

Acknowledgements

Notes and references

1. H. P. Dhar, L. G. Christner and A. K. Kush, *Journal of the Electrochemical Society*, 1987, **134**, 3021-3026.
2. N. Iwasa, S. Masuda, N. Ogawa and N. Takezawa, *Applied Catalysis A-General*, 1995, **125**, 145-157.
3. H. Zhang, J. M. Sun, V. L. Dagle, B. Halevi, A. K. Datye and Y. Wang, *ACS Catalysis*, 2014, **4,** 2379-2386.
4. M. Armbruster, M. Behrens, K. Fottinger, M. Friedrich, E. Gaudry, S. K. Matam and H. R. Sharma, *Catalysis Reviews-Science and Engineering*, 2013, **55**, 289-367.
5. N. Iwasa, S. Masuda and N. Takezawa, *Reaction Kinetics and Catalysis Letters*, 1995, **55**, 349-353.
6. N. Iwasa, T. Mayanagi, N. Ogawa, K. Sakata and N. Takezawa, *Catalysis Letters*, 1998, **54**, 119-123.
7. M. Friedrich, S. Penner, M. Heggen and M. Armbruster, *Angewandte Chemie-International Edition*, 2013, **52**, 4389-4392.
8. M. Heggen, S. Penner, M. Friedrich, R. E. Dunin-Borkowski and M. Armbruster, *Journal of Physical Chemistry C*, 2016, **120**, 10460-10465.
9. Y. H. Chin, Y. Wang, R. A. Dagle and X. H. S. Li, *Fuel Processing Technology*, 2003, **83,** 193-201.
10. N. Iwasa, T. Mayanagi, W. Nomura, M. Arai and N. Takezawa, *Applied Catalysis A-General*, 2003, **248**, 153-160.
11. N. Iwasa, S. Kudo, H. Takahashi, S. Masuda and N. Takezawa, *Catalysis Letters*, 1993, **19**, 211-216.
12. T. Conant, A. M. Karim, V. Lebarbier, Y. Wang, F. Girgsdies, R. Schlogl and A. Datye, *Journal of Catalysis*, 2008, **257**, 64-70.
13. G. Xiong, L. Luo, C. Li and X. Yang, *Energy & Fuels*, 2009, **23**, 1342-1346.
14. M. Sankar, Q. He, M. Morad, J. Pritchard, S. J. Freakley, J. K. Edwards, S. H. Taylor, D. J. Morgan, A. F. Carley, D. W. Knight, C. J. Kiely and G. J. Hutchings, *ACS Nano*, 2012, **6**, 6600-6613.
15. M. Morad, M. Sankar, E. H. Cao, E. Nowicka, T. E. Davies, P. J. Miedziak, D. J. Morgan, D. W. Knight, D. Bethell, A. Gavriilidis and G. J. Hutchings, *Catalysis Science & Technology*, 2014, **4**, 3120-3128.
16. H. Bahruji, J. R. Esquius, M. Bowker, G. Hutchings, R. D. Armstrong, W. Jones, *Topics in Catalysis,* 2018*,* **61***,* 144-153.
17. NIST X-ray Photoelectron Spectroscopy Database, Version 4.1 in National Institute of Standards and Technology, Gaithersburg, 2012.
18. H. Lorenz, M. Friedrich, M. Armbruster, B. Klotzer and S. Penner, *Journal of Catalysis*, 2013, 297, 151-154.
19. G. W. Xiong, L. T. Luo, C. Q. Li and X. M. Yang, *Energy & Fuels*, 2009, **23**, 1342-1346.
20. A. M. Karim, T. Conant and A. K. Datye, *Physical Chemistry Chemical Physics*, 2008, **10**, 5584-5590.
21. N. Iwasa, N. Takezawa, *Topics in Catalysis,* 2003, **22,** 215-224.
22. H. Nowotny and H. Bittner, *Monatshefte Fur Chemie*, 1950, **81**, 679-680.
23. C. Rameshan, C. Weilach, W. Stadlmayr, S. Penner, H. Lorenz, M. Havecker, R. Blume, T. Rocha, D. Teschner, A. Knop-Gericke, R. Schlogl, D. Zemlyanov, N. Memmel, G. Rupprechter and B. Klotzer, *Journal of Catalysis*, 2010, **276**, 101-113.
24. M. Lenarda, E. Moretti, L. Storaro, P. Patrono, F. Pinzari, E. Rodriguez-Castellon, A. Jimenez-Lopez, G. Busca, E. Finocchio, T. Montanari and R. Frattini, *Applied Catalysis A-General*, 2006, **312**, 220-228.
25. J. A. Rodriguez, *Journal of Physical Chemistry*, 1994, **98**, 5758-5764.
26. H. Bahruji, M. Bowker, G. Hutchings, N. Dimitratos, P. Wells, E. Gibson, W. Jones, C. Brookes, D. Morgan and G. Lalev, *Journal of Catalysis*, 2016, **343**, 133-146.
27. F. Cocco, B. Elsener, M. Fantauzzi, D. Atzei and A. Rossi, *RSC Advances*, 2016, **6**, 31277-31289.

Graphical Abstract: